Charge and fluence lifetime measurements of a dc high voltage GaAs photogun at high average current

J. Grames, R. Suleiman, P. A. Adderley, J. Clark, J. Hansknecht, D. Machie, M. Poelker, and M. L. Stutzman
Thomas Jefferson National Accelerator Facility, Newport News, Virginia 23606, USA
(Received 17 December 2010; published 20 April 2011)

GaAs-based dc high voltage photoguns used at accelerators with extensive user programs must exhibit long photocathode operating lifetime. Achieving this goal represents a significant challenge for proposed high average current facilities that must operate at tens of milliamperes or more. This paper describes techniques to maintain good vacuum while delivering beam, and techniques that minimize the ill effects of ion bombardment, the dominant mechanism that reduces photocathode yield of a GaAs-based dc high voltage photogun. Experimental results presented here demonstrate enhanced lifetime at high beam currents by: (a) operating with the drive laser beam positioned away from the electrostatic center of the photocathode, (b) limiting the photocathode active area to eliminate photoemission from regions of the photocathode that do not support efficient beam delivery, (c) using a large drive laser beam to distribute ion damage over a larger area, and (d) by applying a relatively low bias voltage to the anode to repel ions created within the downstream beam line. A combination of these techniques provided the best total charge extracted lifetimes in excess of 1000 C at dc beam currents up to 9.5 mA, using green light illumination of bulk GaAs inside a 100 kV photogun.

DOI: 10.1103/PhysRevSTAB.14.043501 PACS numbers: 29.27.Hj, 29.25.Bx, 41.75.Fr

I. INTRODUCTION

The photocathode lifetime of modern dc high voltage GaAs photoguns is limited primarily by ion bombardment [1], the mechanism where residual gas is ionized by the extracted electron beam and transported backward to the photocathode where the ions adversely affect photocathode yield commonly referred to as quantum efficiency (QE). Video 1 shows an animation of ion bombardment within the dc high voltage continuous electron beam accelerator facility (CEBAF) photogun, with the electron beam originating at or away from the electrostatic center (EC), defined as the axis formed by the cathode and anode. The electron beam is focused by the electrode geometry toward the EC as it is accelerated to the anode. Gas molecules entering the electron beam path may be ionized [2,3] and similarly accelerated, but toward the cathode and along a less deflected path due to their greater mass. Consequently, ions are delivered to the photocathode along a ''trench'' that begins at the point of photoemission and leads toward the EC [Fig. 1]. The rate of ion production depends strongly on the electron beam energy as shown in Fig. 2 for molecular hydrogen, the prevalent species in a photogun. The maximum ion production rate is expected to correspond to the lowest energy electrons very near the photocathode surface; however, measurements indicate ions of all energy (at least up to 100 keV, the maximum energy studied in this paper) contribute to diminished QE.

The mechanisms by which impinging ions reduce QE is the subject of ongoing speculation. While it has been determined that ions with sufficient kinetic energy penetrate the surface of the photocathode [4], it is not known what these ions do to the photocathode. They might damage the GaAs crystal structure or serve as trapped interstitial defects that reduce the electron diffusion length or serve as unwanted dopant species, adversely altering the

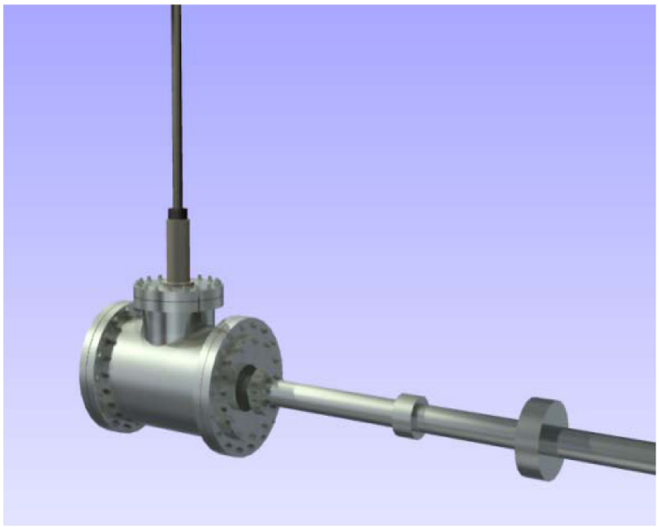

VIDEO 1. Animated sequence of ion bombardment for typical electron photoemission in a dc high voltage GaAs photogun.

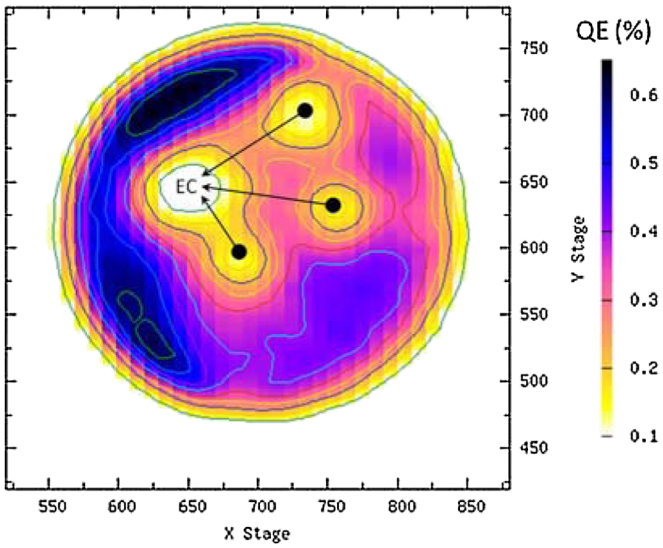

FIG. 1. QE measured across the surface of a strained superlattice GaAs photocathode used at CEBAF that has been damaged by ions. The electron beam was extracted from three different radial locations. Note QE ''trenches'' that terminate at a common ''electrostatic center (EC).''

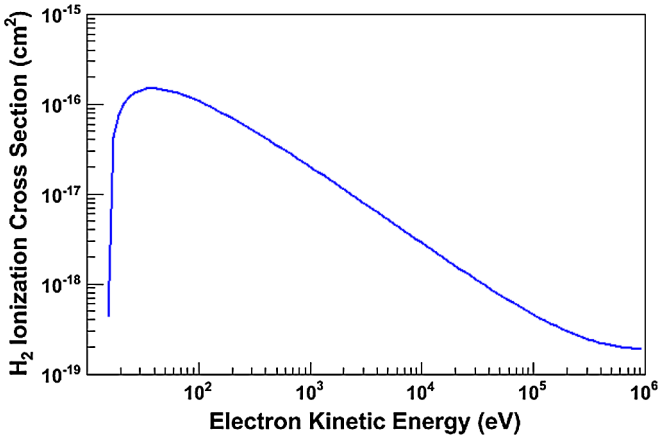

FIG. 2. Electron impact ionization cross section for H_2 [21], the dominant gas species inside a modern baked ultrahigh vacuum (UHV) dc high voltage photogun, as a function of electron kinetic energy.

photocathode energy band structure. Impinging ions might also sputter away the chemicals used to reduce the work function at the surface of the photocathode. Predicting which ions are the most problematic (gas species and energy) awaits a detailed modeling study that considers many parameters including: relevant ion species with appropriate ionization cross sections, accurate trajectories of both ions and electrons, sputtering yield of alkali (cesium) and oxidant (fluorine) used to create the negative electron affinity (NEA) condition at the photocathode surface required for photoemission, and stopping depths of ions within the photocathode. Parameters such as optical absorption length, electron diffusion length, and active layer thickness (especially for high polarization photocathodes) are likely to be important factors, too.

Regardless of how ions degrade QE, maintaining and improving the gun vacuum is the most direct way to suppress the problem of ion bombardment and thereby prolong photocathode operating lifetime. Methods to improve static vacuum inside the gun include enhancing the pump speed in the vicinity of the photocathode, improving the vacuum of the adjoining beam line, and reducing the gas load inside the photogun, for example by reducing the surface area of the gun structure or via a prolonged high temperature bake of the gun vacuum chamber material to reduce outgassing rate [5]. All of the present dc high voltage GaAs polarized photoguns rely on nonevaporable getter (NEG) and ion pump technologies, where the ion pump serves to pump those species not efficiently pumped by the NEG such as methane, carbon monoxide, and helium. For example, it is widely known that ion pump speed falls as the system pressure drops below 1×10^{-10} Torr, so it is possible the ion pump represents a source of gas (rather than a pump) in these systems. Perhaps alternatives to these pumps are required to improve vacuum below the typical mid-10^{-12} Torr pressure observed today. For example, 2 K cryopumping (cryocondensation) or 4 K cryotrapping (cryosorption) might provide better vacuum although it is not entirely obvious what NEG pump deficiency the cryopump may overcome.

On the dynamic vacuum front (i.e., vacuum while operating the gun at high voltage), it is extremely important to eliminate field emission from the high voltage cathode electrode and support structure, which can degrade vacuum via electron stimulated desorption and subsequent ion bombardment and chemical poisoning of the photocathode. In addition, it is extremely important to effectively ''manage'' all extracted beam leaving the photocathode, including beam not intentionally produced, for example, from extraneous laser reflections or background light illuminating the activated surface of the photocathode (the subject of more discussion below).

Although not a replacement for vacuum research and development, this paper demonstrates it is also possible to extend the operating lifetime of the photocathode by relatively simple means, including: (a) operating with the drive laser beam positioned away from the electrostatic center of the photocathode, (b) limiting the photocathode active area to eliminate photoemission from regions of the photocathode that do not support efficient beam delivery, (c) using a large drive laser beam to distribute the offending ions over a broader area, and, finally, (d) by applying a relatively low bias voltage to the anode to repel ions created within the downstream beam line. All results were obtained at average beam current greater than 0.5 mA, with unpolarized beam extracted from bulk GaAs photocathodes using dc green light (532 nm). A combination of these

techniques provided the best charge lifetime in excess of 1000 C at dc average current up to 9.5 mA, where charge lifetime describes the number of coulombs of electrons that can be extracted from the photocathode before photocathode QE at the laser spot location falls to $1/e$ ($\sim 37\%$) of the initial value. Granted, some of these techniques (a and c) degrade emittance, but the benefits of longer photogun operating lifetime might warrant their implementation.

It is worthwhile to discuss the different lifetime metrics discussed in this paper: operational lifetime and charge lifetime. Operational lifetime is simply the amount of time the photogun can satisfy the accelerator beam current requirements. This is a very practical metric but since accelerator beam specifications can vary significantly from one accelerator to another (e.g., average current, duty factor, days/week of operation), it is often ill-suited for making comparisons of photoguns at different labs. Charge lifetime is defined as the amount of charge that can be extracted from a photocathode before QE falls to $1/e$ of its initial value. Of course, the photogun can continue to operate beyond its charge lifetime if the drive laser is sufficiently powerful. Charge lifetime is a useful metric for conducting analytical studies of a particular photogun but, as will be illustrated below, it depends on many parameters. As such, it too is not always the best metric for comparing one photogun against another. This paper discusses the concept of fluence lifetime as a potentially useful metric that could serve to represent the intrinsic performance of the photogun, independent of the many variables that complicate a global comparison of photoguns.

This paper serves to summarize work conducted over a number of years and reported in segments at workshops and conferences [6]. It is often difficult to accurately deduce cause and effect when operating dc high voltage GaAs photoguns, because so many factors can influence the results. However, these measurements convincingly illustrate the dynamics of four mechanisms that contribute to QE decay. Suggestions for improvements and future experiments are briefly discussed. These results could especially benefit high current accelerator requirements for energy recovery linacs [7], free electron lasers [8], electron cooling of ion beams [9], or the proposed eRHIC Electron Ion Collider [10].

II. LOAD-LOCK PHOTOGUN

Lifetime measurements were performed as part of a lengthy commissioning program for the continuous electron beam accelerator facility (CEBAF) load-lock photogun, where the term ''load-lock'' refers to a multichambered vacuum apparatus that allows the installation of new photocathode samples without lengthy vacuum bakeouts of the entire gun. Each vacuum chamber is isolated from the others by valves, with vacuum improving from one chamber to the next and the best vacuum obtained inside the gun high voltage chamber.

The CEBAF load-locked gun has undergone design changes since its inception; however, the basic overall design was consistent throughout the measurement period described here. The CEBAF load-locked gun consists of four vacuum chambers (Fig. 3) separated by bakable all-metal gate valves with 4.5-inch ConFlat flanges and 2.5-inch inner bore. Three of the chambers remain continually connected: a high voltage chamber for generating the photoemitted electron beam, a preparation chamber for heating and activating photocathodes, and a small-volume intermediary loading chamber that is evacuated and baked with heat tapes when a fourth chamber, the ''Suitcase'', is attached for transferring photocathodes to/from the photogun.

Two styles of gun high voltage chamber were used (Fig. 4): one with a large-bore ceramic insulator [11], and the other with a compact ''inverted'' insulator [12]. Both gun geometries utilize a ''side-ceramic'' approach with the insulator oriented perpendicular to the electron beam path and with photocathode samples inserted from behind into the hollow cathode electrode with 25° focusing angle and flat anode. Both designs have similar cathode-anode electrode shapes at the vicinity of photocathode that provide similar electrostatic focusing appropriate for CEBAF beam conditions (100 μA average current,

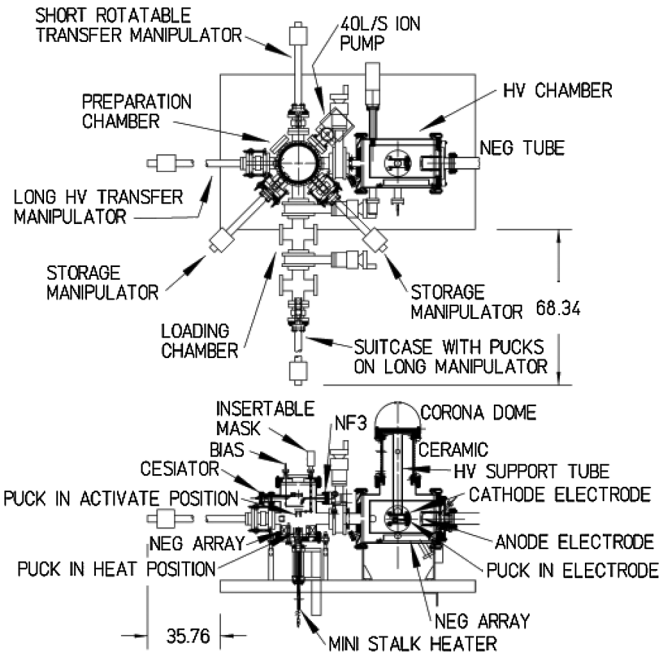

FIG. 3. (Top) Plan view shows the complete gun assembly with four vacuum chambers: gun high voltage chamber (large-bore ceramic insulator design), preparation chamber, intermediary chamber, and Suitcase. (Bottom) Side view shows some of the components inside the preparation chamber including a heater that also serves to move the puck toward a mask used to selectively activate only the center portion of the photocathode.

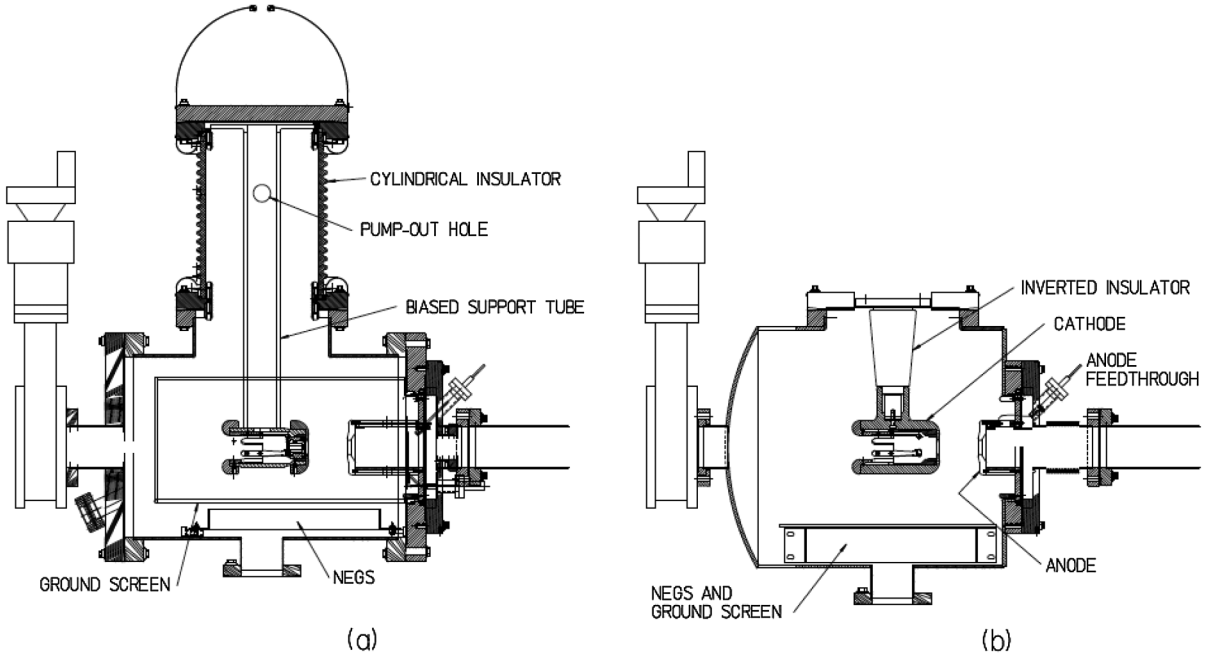

FIG. 4. Diagrams of the load-locked gun high voltage vacuum chambers: (a) conventional large-bore cylindrical insulator and (b) inverted gun with compact tapered insulator that extends into the gun vacuum vessel. Both drawings have the same scale with top flanges 10-inch diameter. The cathode-anode separation is ~6 cm for both designs.

499 MHz pulse repetition rate, and 0.13 pC bunch charge emitted by approximately 50 ps long optical pulse), although the measurements described here were performed with dc beam at milliampere average currents. Both gun styles rely on vacuum pumping using NEG and ion pumps, with NEG pumps (SAES getters WP950 or WP1250) lining the bottom and sides of the high voltage chamber. The inverted gun design provided slightly better vacuum as indicated by a Leybold extractor gauge 6×10^{-12} Torr (nitrogen equivalent value and with valve to the beam line opened) compared to 8×10^{-12} Torr measured on the gun with a conventional cylindrical insulator. Gun vacuum decreases by a few parts in 10^{-12} Torr when the gun vacuum is closed to the beam line. Measurements of lifetime dependence on radial position of the drive laser beam at the photocathode, and photocathode active area, were performed using the inverted gun geometry. Measurements of lifetime dependence on drive laser beam spot size, and with a biased anode, were performed using the photogun with large-bore cylindrical insulator.

The anode electrode for both gun designs was electrically isolated from the grounded high voltage chamber using a thin ceramic spacer and attached to a sensitive current meter to detect field emission and/or photoemission from the edge of the photocathode. In addition, this feature provided a means to bias the anode at relatively low voltage, to repel ions generated downstream of the anode from entering the cathode-anode gap.

Key features of the preparation chamber include: storage for up to four pucks (each puck supports one photocathode), a mask for selective activation of a portion of the photocathode surface, puck heating to at least 600°C and good vacuum obtained using NEG and ion pumps. Photocathode activation takes place with cesium by resistively heated dispensers from SAES getters and NF_3 by a leak valve from a small reservoir. The preparation chamber has four magnetically coupled sample manipulators: one long manipulator with translation and rotation capability for moving pucks into or out of the gun high voltage chamber cathode electrode, one short manipulator with translation and rotation capability for moving pucks from/onto the heater assembly as well as to transferring pucks to/from the long manipulator, and two short manipulators with translation capability that serve to hold pucks with additional photocathode samples. Care must be taken during the initial commissioning bake of the preparation chamber—the magnetic manipulators can develop excessive friction that limits functionality when heated above ~200°C. Each magnetic manipulator is attached to a bellows assembly with adjustment screws for proper alignment to the electrode, heater, and other manipulators. Pumping inside the prep chamber was provided by a 40 L/s ion pump and 1.5 SAES getters WP-1250 NEG modules with support rods removed, and coiled into the bottom of the vacuum chamber. Pressure in the preparation chamber was $\sim 1 \times 10^{-10}$ Torr.

The photocathode samples were indium-soldered to cup-shaped molybdenum pucks (Fig. 5), similar to the SLAC design [13]. The reentrant cup accommodates either a heater element or a mechanical manipulator. The puck and manipulator are keyed to aid extracting the puck from the electrode. The pucks must have a relatively smooth

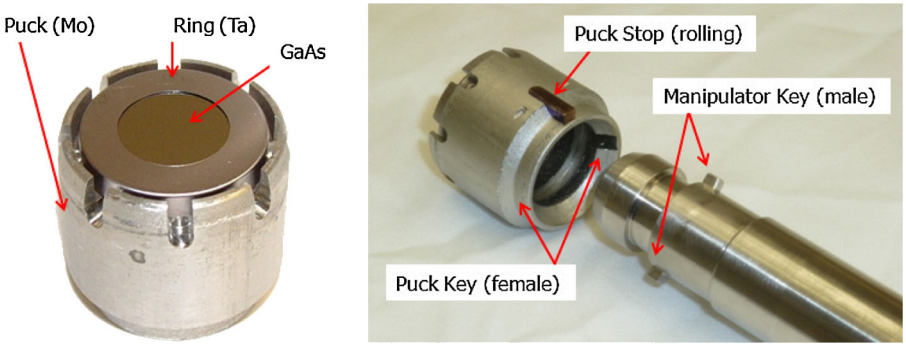

FIG. 5. (Left) Photocathode attached to a puck and (right) the tip of the long manipulator being inserted into the rear of the puck (right).

outer surface to prevent binding inside the electrode, and a smooth inner surface to ensure good mechanical contact to the heater. A small ''ear'' was added to the outer surface of the puck, to prevent it from rolling off manipulators, and to prevent it from rotating inside the electrode when extracting the photocathode from the high voltage chamber.

To activate a photocathode, a puck with GaAs photocathode located on one of the two magnetically coupled storage manipulators was inserted to a position above the heater located at the center of the preparation chamber. The heater was then raised into the puck capturing it, and finally the storage manipulator was retracted to the original position. The heater was then lowered such that the puck was positioned inside a stainless steel sleeve at the bottom of the preparation chamber, which serves to keep other portions of the preparation chamber cool during puck heating. After a typical 2 h soak at ~550°C, the puck was allowed to cool to room temperature. Water-cooled copper ''fingers'' can be moved into contact with the puck to reduce the cooling time from 8 to 4 hours. Once the puck temperature fell below ~30°C, the puck was moved upward to contact an aluminum mask with two different holes (5 and 7 mm diameter holes) that limit the active area of the photocathode by protecting all but the area visible through the hole from the cesium deposition [14]. The mask can also be moved aside to activate the entire surface of the photocathode (12.8 mm diameter). Cesium and nitrogen trifluoride (NF_3) were applied in a ''yo-yo'' manner while monitoring photocurrent with a positively biased ~300 V anode ring. After activation, the vacuum quickly recovered and the puck was transferred to the long manipulator for installation into the gun high voltage chamber. The total time for heating, cooling, and activation was approximately ten hours.

To reduce the overall footprint and provide a means to deliver pucks to the photogun at CEBAF, a suitcase approach was adopted. The suitcase mates to the gun only when new pucks/photocathodes are needed. When not in use the suitcase is maintained under vacuum separated from the photogun. The suitcase includes a bakable all-metal valve, a 25 L/s ion pump, and a sample holder that can accommodate four pucks, and the suitcase in combination with the two storage manipulators allows the transfer of all four pucks into and out of the suitcase during one installation.

To use the suitcase, a small intermediary chamber must be evacuated and baked, before valves to the preparation chamber and suitcase can be opened. This intermediary chamber is simply a four-way cross that includes a 40 L/s ion pump with pump-out port. Resistive ''heating tapes'' are used to heat the chamber to 250°C for about eight hours, to achieve vacuum $\sim 1 \times 10^{-10}$ Torr. Experience indicates this is adequate—the preparation chamber vacuum is not degraded following the puck transfer and photocathodes exhibit high QE (bulk GaAs QE ~20% at 532 nm, spin polarized superlattice GaAs QE ~1% at 780 nm).

III. DIAGNOSTICS BEAM LINE

The load-locked gun was attached to a dedicated ultrahigh vacuum (UHV) beam line (Fig. 6) ~5 m long. The beam line was baked at 250°C for 30 hours, with the exception of the Faraday cup at the end of the beam line, which was baked at 450°C for 24 hours, to reduce outgassing during high current operation. Two differential pump stations each with four SAES getter WP1250 modules using ST707 material provide a factor of about 100 vacuum isolation of the beam dump from the gun [15]. Six diode ion pumps are distributed along the beam line and ion pump current can be monitored on a nanoampere level using sensitive current meters within the ion pump high voltage supply [16]. This vacuum diagnostic serves as a sensitive electron beam loss monitor and was used to optimize electron beam steering and beam envelope management. For example, intercepted current as small as 50–100 pA on an electrically isolated anode in the gun chamber can be resolved by an increase in ion pump supply currents at the gun and along the beam line (see Table I).

The electron beam exits the gun through a large-bore (2.5'') NEG-coated beam pipe and is then deflected 15° by an air-core cosine-theta dipole magnet. The bend allows illumination of the photocathode at normal incidence

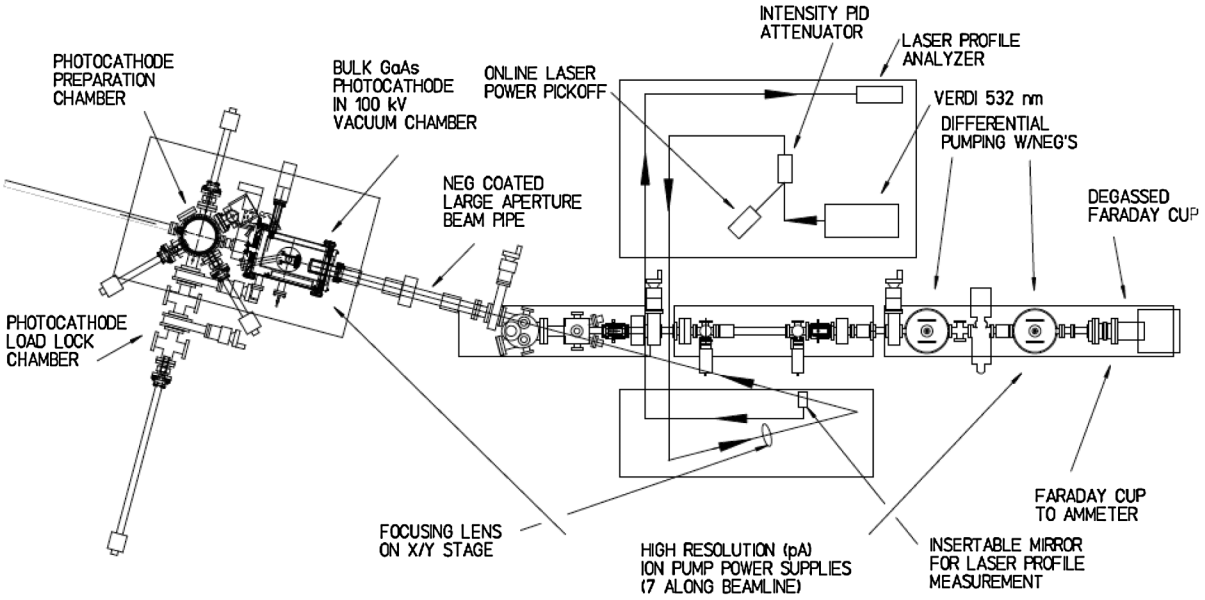

FIG. 6. The 100 kV dc high voltage load-locked GaAs photogun and beam line.

without needing mirrors inside the vacuum chamber. A large portion of the incident laser power ($\sim 30\%$) is reflected from the photocathode due to the high index of refraction of GaAs. To prevent unwanted photoemission from reflections inside the high voltage vacuum chamber, the laser and gun are aligned so that the reflected light exits the laser vacuum window within $\sim 0.1°$ of the incident laser beam. There are four focusing solenoid magnets to manage the beam envelope and numerous steering magnets to keep beam centered in the solenoids and to minimize beam loss in the beam line.

A green light at 532 nm from a frequency-doubled Nd:YVO_4 laser (Coherent Verdi-10) was directed into the vacuum chamber through a vacuum window located near the bend magnet. The drive laser emits dc light, with maximum power set to 1 W for these measurements. The amount of light at the photocathode could be varied with a computer-controlled attenuator that consists of a fixed linear polarizer and rotatable birefringent $\lambda/2$ wave plate. A focal length lens (2 m) placed near the vacuum window of the beam line provided the tightest beam waist at the photocathode about 0.3 mm diameter, Gaussian full-width at half maximum (FWHM). A larger 1.5 mm laser spot was obtained using a 1.5 m focal length. A commercial CCD camera and scanning razor-blade apparatus were used to measure laser profile and spot size and verify the laser beam was circular with Gaussian profile at the corresponding distance to the photocathode. The focusing lens was mounted to an *x*-*y* stepper motor stage to move the laser spot to different locations on the photocathode and to map photocathode QE before and after charge lifetime measurements. The optical elements (mirrors, wave plates, polarizing cubes) were all purchased with appropriate coating for green light.

IV. MILLIAMPERE CHARGE LIFETIME EXPERIMENTS

The experiment consisted of numerous measurements at different beam currents, different radial locations of the laser beam on the photocathode, different photocathode active areas, and different laser spot sizes. Bulk GaAs photocathodes (625 μm thick unstrained GaAs, *p* doped with Zn at $\sim 8 \times 10^{18}$ atoms/cm^3, with 100 plane prepared by cutting and polishing) were used for all measurements. Beam current, drive laser power, and ion pump current at

TABLE I. Summary of conditions as a function of active area.

Beam current (mA)	0	2		
Active diameter (mm)	Any	5	7	12.8
Anode current (pA)	0.0 ± 0.3	0.0 ± 0.3	0.0 ± 0.3	100–1000[a]
Rad monitor (mR/h)	0.006 ± 0.003	0.015 ± 0.005	0.018 ± 0.005	3–7
Gun ion pump (pA)	0	0	0	0–30
Beam line ion pump (nA)	3	3	3	4–20

[a]This is the range of values at the start of the lifetime measurements. The anode current is proportional to the laser power.

seven locations along the beam line were monitored for each run. Beam line focusing and steering magnets were adjusted for each run to minimize electron beam loss, as indicated by sensitive ion pump current monitoring as noted above, and thereby provide the best possible vacuum conditions and consistency for each run. Beam current was maintained constant throughout each run using a generic proportional-integral-derivative software control loop to vary the amount of laser power delivered to the photocathode. The run might take minutes or hours, depending on the conditions of the experiment, and involved making a charge lifetime measurement, defined as the amount of charge that could be extracted from the photocathode until the QE dropped to $1/e$ of the initial starting value (more below). QE degradation across the surface of the photocathode could be monitored following each run by extracting about 1 μA from the photocathode biased at -200 V while scanning the laser across the photocathode using the x/y stepper motor stage. (For the inverted gun, the photocathode was grounded and the anode was biased at $+200$ V.)

V. EXPERIMENT RESULTS—LASER BEAM POSITION AND ACTIVE AREA

One of the most significant breakthroughs in polarized electron source development at Jefferson Lab was the discovery that, in addition to the core electron beam delivered to the experimental halls, the photoguns produced a small amount of unwanted, unintended photoemission from the edge of the photocathode that was not properly transported away from the photogun [11]. These electrons followed extreme trajectories, striking the anode or beam pipe wall near the gun, degrading vacuum via electron stimulated desorption, and hastening QE decay. Initially, this was puzzling because the drive laser beam was always focused to a small spot at the photocathode, typically less than a millimeter in diameter, compared to the full photocathode diameter of 12.8 mm. It was speculated that the unwanted photoemission from the edge of the photocathode was produced by stray, scattered light or via recombination light emitted by the cathode itself, since most of electrons excited to the conduction band merely decay back to the valance band. To eliminate the unwanted photoemission from the edge of the photocathode, a number of steps were taken including installation of a vacuum window with an antireflection coating, and removing apertures from the laser table that produced diffraction rings. But the most dramatic improvement in photocathode lifetime came initially from anodizing the edge of the photocathode, or later using a mechanical mask, to prevent creating the NEA condition for photoemission at photocathode locations that did not support proper beam transport.

To quantify this phenomenon at high average current, lifetime measurements were made using bulk GaAs photocathodes with different active area dimensions (Fig. 7): the entire photocathode (12.8 mm diameter) and smaller areas (5 and 7 mm diameter) obtained using the activation mask inside the preparation chamber. A tightly focused laser beam 0.35 mm diameter Gaussian FWHM was directed at different locations on the photocathode, with 2 mA average beam current delivered to the beam line dump from each location. Lifetime was determined for all runs (Fig. 8), the anode current was monitored to detect the presence of unwanted photoemission from the edge of the photocathode, and an x-ray detector attached to the side of the gun vacuum chamber served as an additional beam loss diagnostic (see Table I).

When the entire photocathode was activated (12.8 mm diameter), unwanted photoemission from the edge of the photocathode was always detected at the anode (100–1000 pA), correlated with x-ray production significantly above background. When the drive laser beam was positioned at/near the electrostatic center, photocathode charge lifetime was poor, just about 10 C, but improved for positions away from the EC, reaching values between 100 and 200 C at radial locations extending from 1 to 6 mm from the EC.

As expected from experience at CEBAF, selective activation of just a portion of the photocathode (5 and 7 mm), served to eliminate unwanted photoemission from the edge of the photocathode. The anode current was zero to within 0.1 pA, and there was markedly reduced x-ray production. Lifetime values were still poor at the EC, but improved as the laser beam was moved outward from the electrostatic axis. Charge lifetime values reached 300 C for the 7 mm activation and exceeded 600 C for the 5 mm activation.

The radial component of the electrostatic field within the cathode-anode gap is zero along the EC, and grows with radial position. Consequently, electrons leaving the photocathode near the EC follow a relatively straight path, while those emitted at larger radius move toward the electrostatic axis while traversing the gap. Similarly, a positively charged gas ion will also experience the radial electric field; however, being significantly more massive will follow a nearly normal path connecting the point of ionization to the photocathode. The total ion dose will then be extended from the point of laser illumination back to the EC, with the highest energy ions contributing from ionization furthest from the photocathode, consequently closest to the EC. Therefore, it makes sense that lifetime would be poor when the point of photoemission and the EC coincide, and that lifetime would improve as laser beam moved away.

A smaller active area means there are fewer extraneously emitted electrons traveling extreme trajectories, striking surfaces and degrading vacuum; however, to the extent that one can efficiently transport all extracted electrons, Fig. 8 suggests that photoemission away from the EC

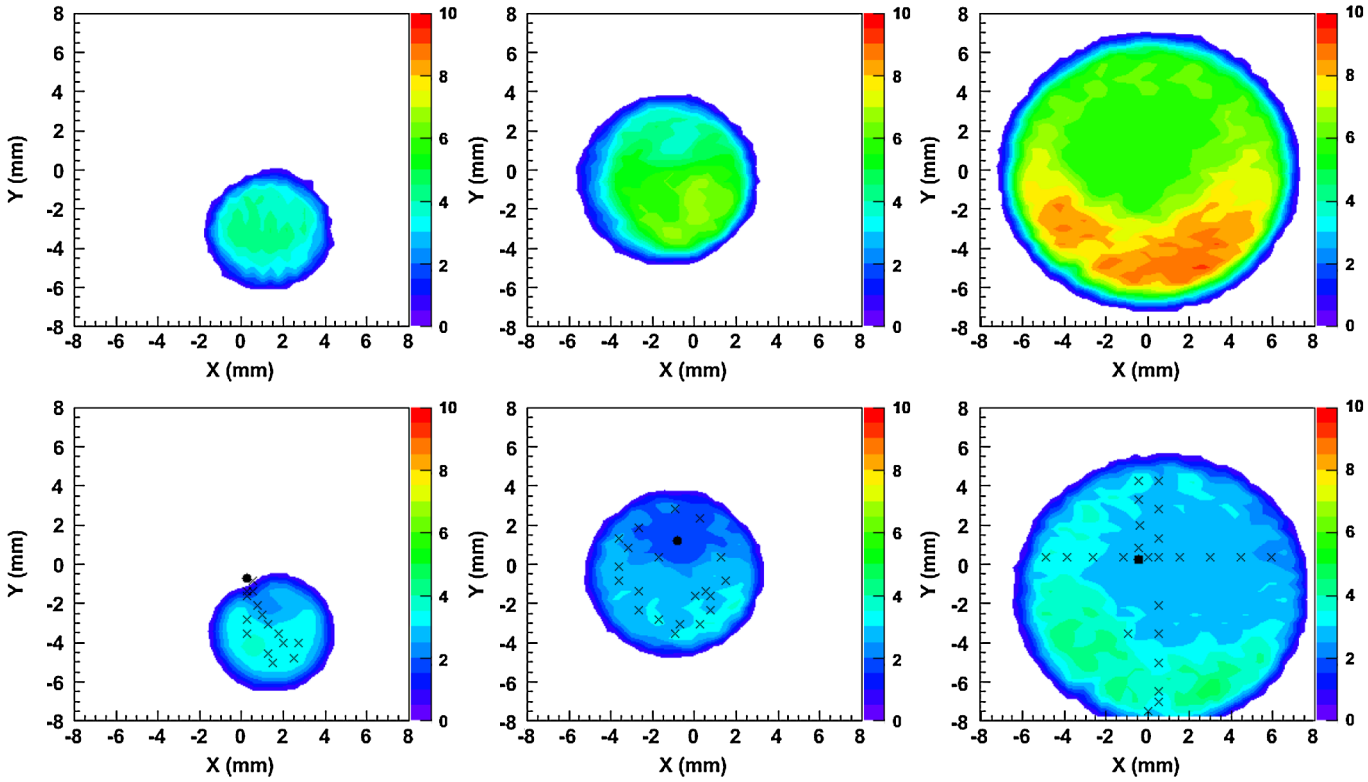

FIG. 7. False color images of photocathode QE after activation (upper) and after completing the lifetime measurements (lower) for the 5, 7, and 12.8 mm diameter activations, respectively. The crosses indicate location of each lifetime measurement and the filled circle is the estimated EC.

is beneficial. For applications with large laser beams, it would be wise to revisit the cathode-anode design to ensure more efficient beam transport from locations across the entire photocathode surface.

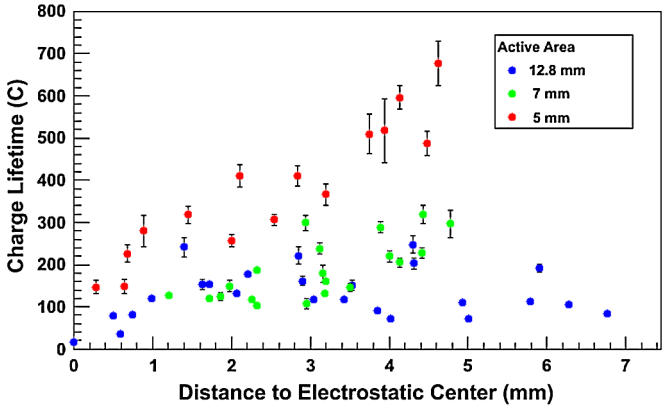

FIG. 8. The photocathode charge lifetime versus radial position of the drive laser beam relative to the photocathode electrostatic center and as a function of photocathode active area diameter: 5, 7 and 12.8 mm. The size of the error bar is related to the quality of the exponential fit to the photocathode QE decay. The best exponential fits (and smallest error bars) were obtained when QE decayed quickly, with charge extracted comparable to the charge lifetime.

VI. EXPERIMENT RESULTS—LASER SPOT SIZE

Beam current and vacuum are widely appreciated to be important factors that influence photogun lifetime as these parameters directly relate to how many ions are produced. Less appreciated is the impact of the size of the laser beam on photogun lifetime. Consider that the same number of ions will be produced within the cathode-anode gap regardless if the drive laser beam was big or small, but for a larger laser beam, the ions will be distributed over a larger area and QE should decrease more slowly. With this in mind, Sinclair first proposed the concept of fluence lifetime [17]—the amount of charge that could be extracted *per unit area* before QE falls to $1/e$ of its original value, and that fluence lifetime would be a constant for each photogun. Furthermore, the fluence lifetime of a gun measured with a small laser spot could be used to predict the charge lifetime of a gun illuminated with a large laser spot.

To test the validity of this hypothesis, lifetime measurements were made over a broad range of currents (0.5 to 9.5 mA) by illuminating a freshly activated photocathode with 5 mm active area, with small and large laser beams -0.32 and 1.55 mm. A prediction based on constant fluence lifetime suggests charge lifetime would scale by the ratio of the two laser beam areas, corresponding to a charge lifetime enhancement of 23 for the larger laser spot size. The results shown in Fig. 9 clearly indicate an

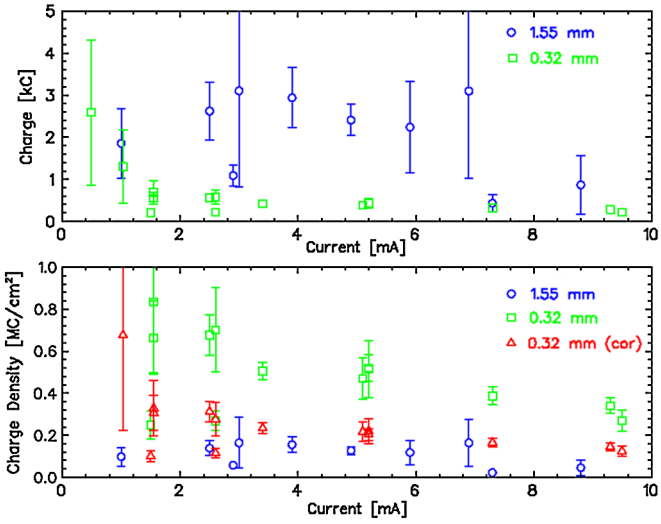

FIG. 9. (Top) Measured charge lifetime vs average beam current for small and large laser spots, and (bottom) fluence lifetime vs average beam current for the two laser spot sizes. Red data points correspond to measurements corrected for radial dependence, see text.

improved charge lifetime when using the larger laser spot, but charge lifetime increased by only a factor of 6. There is significantly better agreement between measurement and prediction when the radial position of laser beam is considered. Note that small laser spot data were collected from four locations 4.8–6.0 mm from the EC, while the large laser spot data were collected from a location 1.8—2.1 mm from the EC (see Fig. 10). When the small spot results are ''corrected'' (red data points) to account for operation from a further radial position—by reducing the lifetime values by 30%, using the results of the previous section and shown in Fig. 8—fluence lifetime values are comparable for both data sets, between 0.1–0.3 $\times$ 10^6 C/cm^2.

The total charge collected for each run was typically 10–50 C. As in Fig. 8, the error bars assigned to data points in Fig. 9 are related to the quality of the exponential fit to the photocathode QE decay. Large error bars correspond to runs that exhibited large charge lifetime performance, where QE decayed very little throughout the duration of the measurement. Ideally, the charge extracted would be comparable to the charge lifetime value, but for the large laser spot measurements this was not practical, as a run might require days of beam delivery. Specifically, it was difficult to maintain constant operating conditions throughout a days-long run. Subtle, untracked, variations might have a large impact on a given charge lifetime result, for example, if laser pointing instability occurred and was not known.

VII. EXPERIMENT RESULTS—BIASED ANODE

Residual gas can be ionized and trapped by the electron beam. Rejecting these ions from reaching the cathode is not a new subject [18], however, the cross section for ionization in modern high voltage photoguns is small, and so until recently [19] the ions created downstream of the anode had largely been ignored by photogun community. Yet, those that do will be delivered to the photocathode EC at the full gun voltage. Consider a 100 keV electron beam produced within a 6 cm cathode-anode gap at a pressure of 5 $\times$ 10^{-12} Torr dominated by H_2. The integrated ion production within the gap will be 15 000 ions every second per milliampere of electron beam current. A comparable number of ions will be produced downstream of the anode over 100 cm of the beam line. Even more ions will be

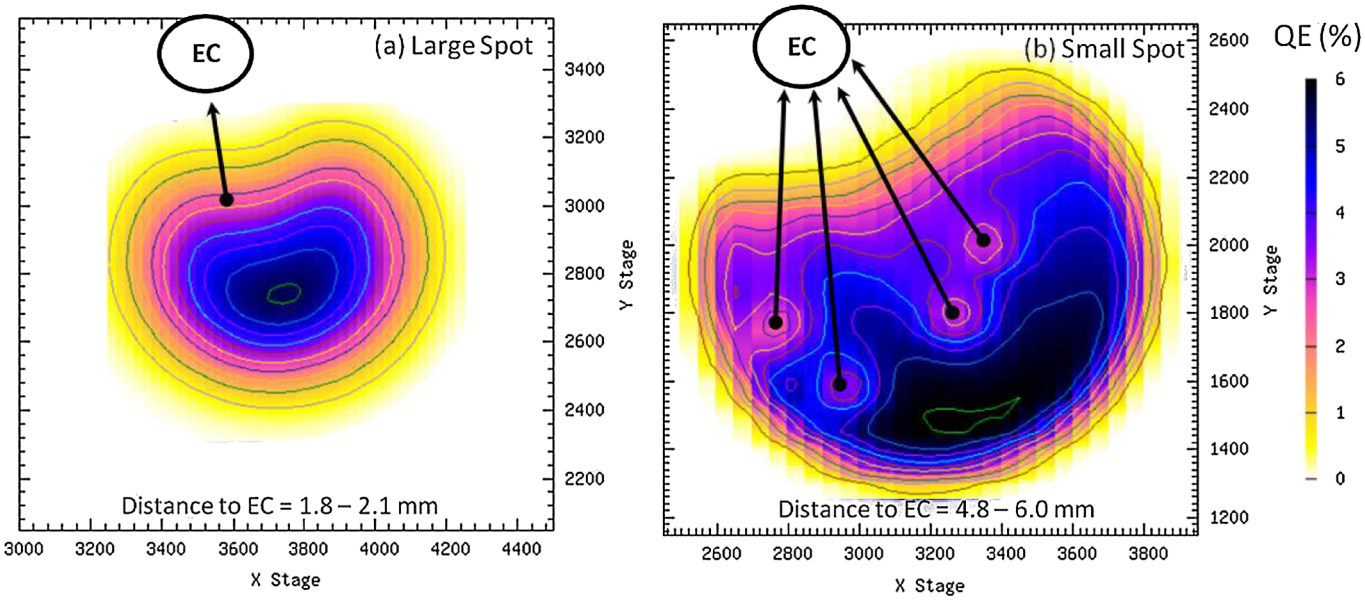

FIG. 10. False color plots of photocathode QE after the (a) large and (b) small laser spot size lifetime measurements. The arrows indicate the direction of lowest to highest energy ions, and relative distance, from the laser spot toward the estimated location of the EC.

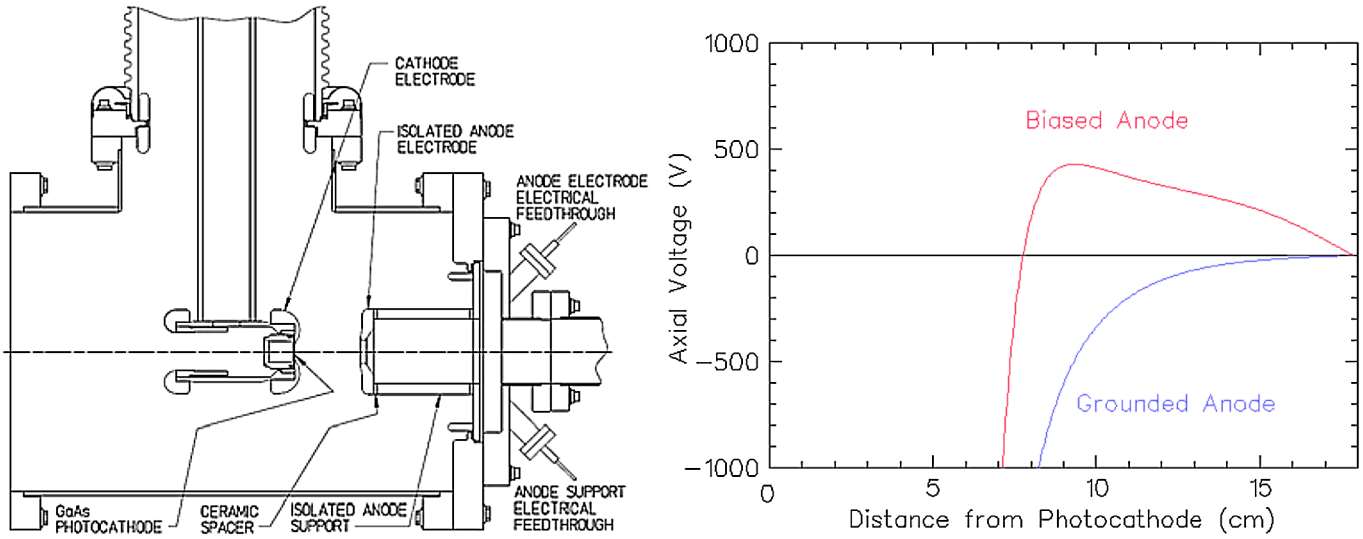

FIG. 11. Modified high voltage chamber assembly (left) and POISSON model (right) showing the potential near the anode (~ 6 cm) to gun exit (~ 18 cm) for the "attractive" grounded (anode electrode = anode support = 0 V) and "barrier" biased (anode electrode = +2000 V, anode support = +300 V) configurations. The potential at the photocathode (distance = 0 cm) is −100 kV, suppressed from the graph.

generated if beam line pressure is worse than the gun pressure, a likely scenario.

An electrostatic barrier is a common means to limit beam trapped ions in accelerators, so it is reasonable to consider applying this to a photogun. To test this idea, we modified the photogun such that the anode and its support were electrically isolated. This allows both to be grounded or electrically biased, determining whether ion production downstream of the anode is a significant factor and whether a potential barrier successfully improves charge lifetime near the EC. The code POISSON [20] was used to model the electrostatic potential of the gun chamber (Fig. 11). Notice the grounded anode configuration attracts positive ions entering the gun chamber toward the photocathode, whereas the biased configuration produces a potential barrier of +425 V, which ions must overcome to enter the cathode-anode gap. This barrier significantly exceeds the kinetic energy of ions trapped within the potential of the electron beam and the final electron energy for both configurations remains 100 keV.

To distinguish QE damage associated with ions created within the cathode-anode gap from those created downstream of the anode, the laser spot (0.32 mm diameter) was moved about 1.8 mm from the EC. Charge lifetime measurements using a 5 mA electron beam indicated about 340 C at the laser spot location for both the grounded and biased anode configurations. However, the correlation of QE degradation at the EC associated with the biased anode is immediately obvious (Fig. 12), suggesting ions are indeed generated downstream of

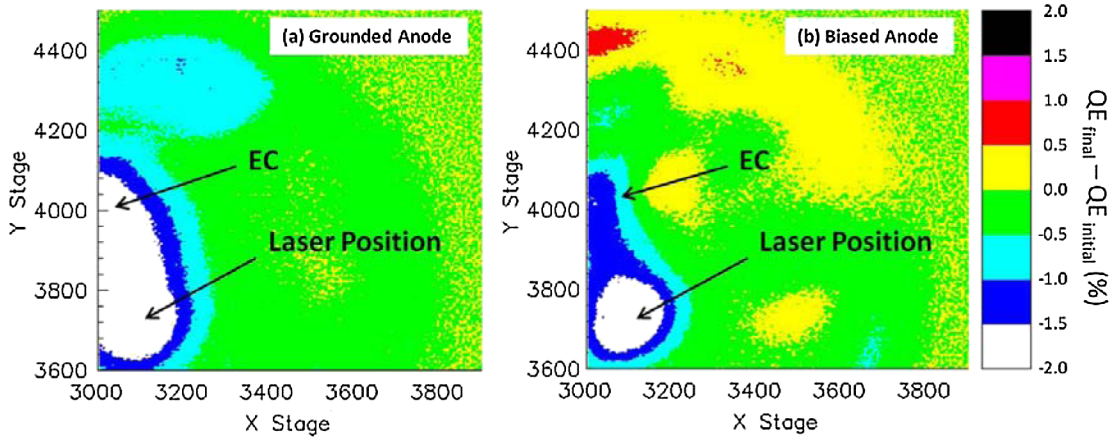

FIG. 12. The change in QE (final–initial) for running with both (a) grounded anode and (b) biased anode configurations is shown. The false color corresponds to the absolute change in QE over the photocathode, notably at the laser spot location ($x = 3100$, $y = 3700$) and EC ($x = 3000$, $y = 4000$).

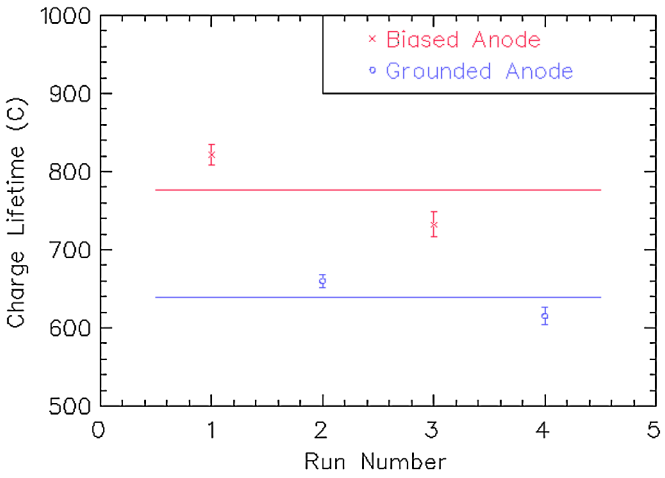

FIG. 13. Photocathode charge lifetime at 2 mA for alternately biased and grounded anode; the average for both the biased and grounded configurations is shown with the horizontal bars. (Note when considering all four data points, there appears to be an overall trend toward reduced charge lifetime, and this may be a result of slight vacuum degradation encountered over the duration.)

the anode and may also be limited with a modest anode bias voltage.

The laser beam was also moved to the EC so that all of the ions generated by the beam, including those within the cathode-anode gap and those downstream of the anode, would accumulate at the EC. The photocathode charge lifetime was measured at a beam current of 2 mA with the anode alternately biased and grounded. The results (Fig. 13) suggest the biased configuration yields an improved lifetime. Averages of the biased and grounded results indicate charge lifetime improved by 22% at the EC, using the biased anode configuration.

VIII. DISCUSSION AND CONCLUSION

The charge lifetime of a bulk GaAs photocathode within a dc high voltage photogun illuminated with dc laser light at 532 nm was observed to depend on a number of different factors, including where the laser beam was positioned relative to the electrostatic center of the photocathode, the active area dimension of the photocathode, the laser spot size, and ion production downstream of the anode. The biggest charge lifetime values were obtained with a large laser spot (1.55 mm Gaussian FWHM) positioned a few millimeters from the electrostatic center, and with just the center portion of the photocathode activated to NEA (5 mm out of 12.8 mm). Charge lifetime values under these conditions were approximately 1000 C at average current up to 9.5 mA.

The concept of fluence lifetime of the photogun was explored and data support the idea that a photogun can be described as having an intrinsic fluence lifetime that can be used to predict charge lifetime values under a variety of conditions including laser position relative to the EC and laser spot size. This metric might provide a useful means to compare one photogun to another, even when they are operated under very different conditions.

Assuming fluence lifetime is an intrinsic value of each photogun, it is worthwhile to use the results of this paper to predict operating lifetime at high current accelerators. Imagine all photoguns can be manufactured to provide 0.1 MC/cm^2 at some location away from the EC, and that this condition holds for operation above 10 mA. Consider an accelerator application that requires 10 mA of unpolarized electron beam—860 C of extracted charge per day—operating continuously for weeks with minimal interruption, and imagine a photocathode with initial QE of 20% at 532 nm and a drive laser with 10 W maximum power delivered to the photocathode, which are realistic assumptions. A GaAs photogun with laser spot size of $\sim$1 mm^2 can operate for five days until QE and laser headroom are exhausted. At this point, something must be done to maintain the desired current, for example: the laser beam could be directed to an unused location of the photocathode (minutes), or the photocathode could be replaced or heated and reactivated (hours). Based on CEBAF experience, this level of downtime seems acceptable for extensive user-based research programs.

At 100 mA, however, with 8640 C extracted each day, the situation is not as favorable. The same initial conditions allow just six hours of operation at 100 mA before exhausting available QE and laser power. Assuming one could increase the laser spot size an order of magnitude with the same fluence lifetime, then one could attempt running a couple of days; however, at the expense of a larger source emittance.

The situation is similarly bleak for polarized beam applications—even at considerably lower current—because high polarization photocathodes provide just 1% QE, and rf-pulsed lasers with required near-infrared wavelengths are less powerful than green-laser counterparts. At 10 mA average current and with a 2 W laser, a photogun with 1000 C charge lifetime can operate for about 7 hours before exhausting QE and laser power. It is reasonable to assume the laser could be moved to fresh photocathode locations multiple times to obtain at least one day of beam delivery before replacing the photocathode; however, this level of interruption is unappealing for a user facility.

Accelerator projects that intend to operate at very high average current will require dedicated R&D to improve the static vacuum within GaAs photoguns. Similarly, continued beam-based research such as described in this paper might shed light on how to prolong operating lifetime while delivering beam. Clearly, the measurements reported in the paper indicate there needs to be greater appreciation for cathode electrode design, in terms of transporting all extracted beam from the photocathode—both wanted and unwanted beam. To the authors' knowledge, most

modeling endeavors associated with photogun electrostatic optics assume beam delivery from the center of the photocathode. In the future, a thorough assessment of gun performance should include beam modeling with intentional off-axis photoemission, and inadvertent photoemission from the entire photocathode active area. Likewise, applications requiring operation from near the EC to achieve best emittance may seek new designs, such as the biased anode to suppress photocathode QE damage located at the EC.

ACKNOWLEDGMENTS

Many people not listed as authors helped interpret results related to lifetime dependence on radial position of the drive laser beam and limiting the active area of the photocathode, including: M. Baylac, B. Dunham, P. Hartmann, R. Kazimi, J. S. Price, P. Rutt, C. K. Sinclair, and M. Steigerwald. This paper was authored by Jefferson Science Associates under U.S. DOE Contract No. DE-AC05-06OR23177 and with funding from the DOE Office of High Energy Physics and the Americas Region ILC R&D program.

[1] K. Aulenbacher *et al.*, SLAC Report No. 432, 1993.
[2] L. J. Kieffer and G. H. Dunn, Rev. Mod. Phys. **38**, 1 (1966).
[3] F. F. Rieke and W. Prepejchal, Phys. Rev. A **6**, 1507 (1972).
[4] M. L. Stutzman and J. Grames, in *Proceedings of the 18th International Spin Physics Symposium*, AIP Conf. Proc. No. 1149 (AIP, New York, 2008), p. 1032.
[5] C. D. Park, S. M. Chung, Xianghong Liu, and Yulin Li, J. Vac. Sci. Technol. A **26**, 1166 (2008).
[6] J. Grames, M. Poelker, P. Adderley, J. Brittian, J. Clark, J. Hansknecht, D. Machie, M. L. Stutzman, and K. Surles-Law, in *Proceedings of the 17th International Spin Physics Symposium*, AIP Conf. Proc. No. 915 (AIP, New York, 2006), p. 1037.
[7] J. A. Crittenden *et al.*, in *Proceedings of the 23rd Particle Accelerator Conference, Vancouver, Canada, 2009* (IEEE, Piscataway, NJ, 2009), MO4PBC03.
[8] A. Todd *et al.*, in *Proceedings of the 20th Particle Accelerator Conference, Portland, OR, 2003* (IEEE, New York, 2003), p. 1294–1296.
[9] S. Nagaitsev *et al.*, Phys. Rev. Lett. **96**, 044801 (2006).
[10] V. Ptitsyn *et al.*, in *Proceedings of the 9th European Particle Accelerator Conference, Lucerne, 2004* (EPS-AG, Lucerne, 2004), p. 923.
[11] C. K. Sinclair, P. A. Adderley, B. M. Dunham, J. C. Hansknecht, P. Hartmann, M. Poelker, J. S. Price, P. M. Rutt, W. J. Schneider, and M. Steigerwald, Phys. Rev. ST Accel. Beams **10** 023501 (2007).
[12] P. A. Adderley, J. Clark, J. Grames, J. Hansknecht, K. Surles-Law, D. Machie, M. Poelker, M. L. Stutzman, and R. Suleiman, Phys. Rev. ST Accel. Beams **13**, 010101 (2010).
[13] R. Alley, H. Aoyagi, J. Clendenin, J. Frisch, C. Garden, E. Hoyt, R. Kirby, L. Klaisner, A. Kulikov, R. Miller, G. Mulhollan, C. Prescott, P. Sáez, D. Schultz, H. Tang, J. Turner, K. Witte, M. Woods, A. D. Yeremian, and M. Zolotorev, Nucl. Instrum. Methods Phys. Res., Sect. A **365**, 1 (1995).
[14] K. Aulenbacher, V. Tioukine, M. Wiessner, and K. Winkler, in *Proceedings of the 15th International Spin Physics Symposium*, AIP Conf. Proc. No. 675 (AIP, New York, 2002), p. 1088.
[15] C. Sinclair (private communication).
[16] J. Hansknecht P. Adderley, M. L. Stutzman, and M. Poelker, in Proceedings of the 18th International Spin Physics Symposium (Ref. [4]), p. 1143.
[17] C. Sinclair, in Proceedings of Snowmass 2001, Snowmass Village, CO, 2001 (Report No. SLAC-R-599), http://www.slac.stanford.edu/econf/C010630/proceedings.shtml.
[18] E. L. Ginzton and B. K. Wadia, Proc. IRE **42**, 1548 (1954).
[19] R. Barday and K. Aulenbacher, in Proceedings of the 17th International Spin Physics Symposium (Ref. [6]), p. 1019.
[20] K. Halbach and R. Holsinger, Part. Accel. **7**, 213 (1976), http://www.slac.stanford.edu/spires/find/hep/www?j=PLACB,7,213.
[21] M. Reiser, *Theory and Design of Charged Particle Beams* (Wiley, New York, 1994).